Comparison of three methods of 2D defect profile reconstruction from MFL signal

ZHANG Ou* and YAN Shuxin

JiangNan Design & Research Institute of Machinery & Electricity, Guiyang 550009, China
**Corresponding Author: 18810387896@163.com*

Submitted: 23/04/2018
Revised: 02/07/2019
Accepted: 08/07/2019

ABSTRACT

Estimating flaw profiles from measurements is a typical inverse problem in magnetic flux leakage (MFL) testing. Defect profile reconstruction implies the reconstruction of defect parameters and profiles based on detected MFL signals, and it is of importance in achieving the MFL inversion. Through establishing the state-space model of the defect profile and the measured MFL signals, this paper formulates the inverse problem as a tracking problem with state and measurement equations. Three state-space methods, i.e., extended Kalman filter (EKF), unscented Kalman filter (UKF), and particle filter (PF), are employed to solve the inversion problem, which is described as the classical discrete-time tracking problem on the basis of state and measurement equations. The results illuminate that the three state-space approaches are effective and feasible ways of MFL inversion. Furthermore, by comparing the reconstruction performances, it can be found that the particle filter-based inversion approach is superior to the other two methods in actualizing MFL inversion owing to its accuracy and robustness against noise.

Keywords: profile reconstruction; magnetic flux leakage; extended Kalman filter; unscented Kalman filter; particle filter.

INTRODUCTION

Magnetic flux leakage (MFL) testing is one of the most widely used techniques in the field of electromagnetic nondestructive evaluation (Priewald et al., 2013) (Sun et al., 2016). In the MFL testing, it is of significance to estimate the defects profile from inspected MFL signals using an efficient solution for an inverse problem (Ravan et al., 2010). The inverse problem means defect information estimated by inversing methods, and it can be classified into shape parameters and the reconstructed defect profile (Smorodinskii et al., 2013) (Mukherjee et al., 2013). This inverse problem is an ill-conditioned issue due to the nonuniqueness of the solution, especially in the existence of noise (Khan et al., 2008).

So far, some researches are carried out on the reconstruction of defect profile from inspected MFL signals. As early as 2002, P. Ramuhalli et al. proposed a neural-network-based inversion algorithm for estimating the defect profiles from measured MFL signals and applied this algorithm to simulated MFL data (Ramuhalli et al., 2002). Xu et al. (2012) presented an improved finite-element neural network implanting a FEM in a neural network structure to solve the forward model in MFL testing, and a conjugate gradient method is used as the learning algorithm. W. H. Han et al. combined the cuckoo search and particle filter to estimate the defect profile from the inspected MFL signals and applied a radial-basis function neural network as a forward model (Han et al., 2016). The combination model of the radial wavelet basis function neural network and kernel partial least squares was proposed in Xu et al. (2013), and it was utilized to multiresolution approximation reconstruction of 2D defect profiles in MFL testing. J. Feng et al. put forward a sensor liftoff modification approach of an MFL signal to increase the estimation performance of the defect

profile, and the proposed approach can improve the signal-to-noise ratio and estimate the profile more accurately (Feng et al., 2017). Lu et al. (2017) proposed an effective approach to reconstruct the arbitrary defect profiles in different velocity conditions and demonstrated that the proposed method can achieve better reconstruction accuracy than the ignoring velocity effect models. An efficient method based on axial MFL level profiles was designed to estimate the defect length in Kandroodi et al. (2017), and this method employed the patterns of signal level profiles in the region corresponding to the defect's area. As can be seen from the above examples, the neural network is the main method for solving the MFL inverse problem. Nevertheless, the neural network-based method has the drawbacks that the precision heavily depends on the training database and is sensitive to noise.

This paper presents three approaches of 2D defect profile reconstruction from detected MFL signals, including extended Kalman filter (EKF), unscented Kalman filter (UKF), and particle filter (PF) approaches. It is unnecessary for the three methods to train the samples so that they are very simple to achieve. The EKF is a simple but powerful approach for the identification of structural parameters, treating the unknown structural parameters as part of the states to be estimated (Pan et al., 2016); therefore, it is widely used in state estimation and fault diagnosis (Delgado-Aguiñaga et al., 2016) (Bonnet et al., 2016). However, the EKF has some well-known weaknesses; for instance, when sampling rate is not high, the filter shows a tendency for instability inherently caused by the linearization involved (Kumar et al., 2011). The UKF is a relatively new member of the Kalman filter family (Astroza et al., 2016) and it is an effective nonlinear filtering method widely applied in parameters prediction and estimation (Li et al., 2016). Unlike EKF, it applies a deterministic sampling approach, called unscented transform, to calculate the current mean and covariance of states. This filter provides a recursive mean for state estimation of any dynamic system from some of the state functions or measured state (Gurung et al., 2016). However, the UKF approach is more computationally intensive than EKF.

It is well known that the PF is a powerful tool based on Monte Carlo simulations and recursive Bayesian estimation, approximating the posterior probability distribution by searching a series of random samples in the state space (Yuan et al., 2011). The PF method has the advantage in dealing with nonlinear or non-Gaussian dynamic systems (Zhou et al., 2016), owing to the fact that any probability distribution can be approximated to any desired accuracy if given sufficient particles (Zuo et al., 2013). The basic PF is subject to the degeneracy problem and can be alleviated by resampling techniques (Gonzales et al., 2015). But the resampling stage will result in the loss of sample validity and diversity, leading to sample impoverishment.

In this paper, the three fore-mentioned methods are applied to reconstruct the defect profile from obtained MFL signals, and the performances of the reconstruction are compared by the evaluation indexes. The inverse problem is formulated as a classical discrete-time tracking problem with state equation and measurement equation; i.e., the sequence of defect profile denotes the state transition model and the inspected MFL signal represents the measurement model. As a result, the state-space model of defect profile and MFL signals is achieved using EKF, UKF, and PF approaches.

THEORY OF FOUNDATIONS

Estimating defect profiles from measurements is a typical inverse problem in electromagnetic nondestructive evaluation. This paper proposes a state-space approach for solving the inverse problems in MFL testing. The approach formulates the inverse problem as a tracking problem with state and measurement equations. Meanwhile, the three filtering methods are applied to reconstruct the defect profile.

State-space model

We present this to model a dynamic state-space problem through using two different equations (Li et al., 2011) (Nobrega et al., 2015), i.e., a state transition equation that is employed to model the evolution of the states with position and a measurement model that relates the measurements to the states at a given position k:

$$x(k+1) = f[x(k)] + w(k) \tag{1}$$

$$z(k) = h[x(k)] + v(k) \tag{2}$$

where $x(k)$ denotes the state of the system, and $z(k)$ is the measurement signal. $w(k)$ represents the process noise supposed Gaussian with zero mean and with variance Q, $v(k)$ denotes the observation noise supposed Gaussian with zero mean and with variance R. $f[\bullet]$ and $h[\bullet]$ are nonlinear functions that model the state transition process and the measurement process, respectively.

The state-space model is similar to the classical discrete-time tracking problem for MFL testing. In this paper, we assume that $x(0:k) = \{x(0), x(1), ..., x(k)\}$ is the sequence of defect depth and $z(0:k) = \{z(0), z(1), ..., z(k)\}$ is the measured value of the MFL signal, as shown in Figure 1. $x(k)$ denotes defect depth and $z(k)$ represents the detected MFL signal at location k. So the dynamic state-space problem can be modelled with two different equations, which are in coincidence with Eq. (1) and Eq. (2).

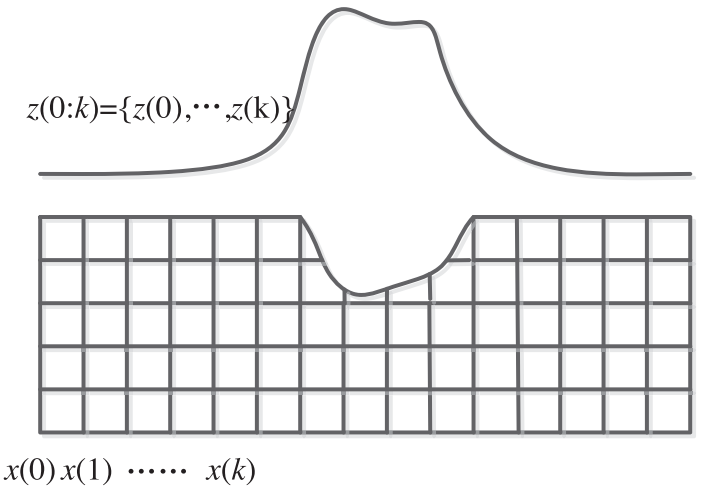

Figure 1. The state-space model of MFL testing.

Extended Kalman Filter

Since the Kalman Filter (KF) is a linear algorithm; it can only guarantee a local convergence of the estimates. However, the EKF is able to give satisfactory results and is a simple but powerful tool for the identification of structural parameters, such as the defect profile reconstruction in nondestructive testing, so it is widely used in state estimation problems (Lindgren, 2015).

In Eq. (1) and Eq. (2), the functions $f[\bullet]$ and $h[\bullet]$ are presented by Taylor series expansions as follows:

$$\begin{cases} f[x(k)] \approx f[\hat{x}(k)] + A(k)[x(k) - \hat{x}(k)] \\ h[x(k)] \approx h[\hat{x}(k)] + H(k)[x(k) - \hat{x}(k)] \end{cases} \tag{3}$$

where

$$A(k) = \left.\frac{\mathrm{d}f}{\mathrm{d}x(k)}\right|_{x(k)=\hat{x}(k)} \tag{4}$$

$$H(k)=\left.\frac{\mathrm{d}h}{\mathrm{d}x(k)}\right|_{x(k)=\hat{x}(k)} \tag{5}$$

The algorithm of the discrete EKF is given as follows (Bressel et al., 2016):

(1) Initialization

$$x(k)=E[x(0)],\ \ P(k)=\mathrm{var}[x(0)]=E\left\{[x(0)-x(k)][x(0)-x(k)]^{T}\right\}$$

(2) Prediction

$$x(k\,|\,k-1)=A(k)x(k-1\,|\,k-1)$$

$$P(k\,|\,k-1)=A(k)P(k-1\,|\,k-1)A^{\mathrm{T}}(k)+Q$$

$$z(k)=H(k)z(k-1\,|\,k-1)$$

(3) Correction

$$K(k)=P(k\,|\,k-1)H^{\mathrm{T}}(k)[H(k)P(k\,|\,k-1)H^{\mathrm{T}}(k)+R]$$

$$P(k)=[I-K(k)H(k)]P(k\,|\,k-1)$$

$$x(k)=x(k\,|\,k-1)+K(k)[z(k)-z(k\,|\,k-1)]$$

Unscented Kalman Filter

Supposing that x is an n-dimensional random variable, its mean is $\overline{x}$ and variance is P. According to the additive noise model in Eq. (1) and Eq. (2), the UKF procedure is as follows (Cang et al., 2015):

(1) Initialization

$$\hat{x}(k)=E[x(0)],\ \ P(k)=\mathrm{var}[x(0)]$$

(2) Calculation of sigma points

The sequence of sigma points is

$$\begin{cases} x^{(0)}=\overline{x} \\ x^{(i)}=\overline{x}+(\sqrt{(n+\lambda)P})_i,\ \ i=1,2,...,n \\ x^{(i)}=\overline{x}-(\sqrt{(n+\lambda)P})_i,\ \ i=n+1,...,2n \end{cases} \tag{6}$$

where $(\sqrt{P})^{\mathrm{T}}(\sqrt{P})=P$, $(\sqrt{P})_i$ is the i-th column of matrix square root.

The weights of sigma point sequence are

$$\begin{cases} \omega_{\mathrm{m}}^{(0)}=\lambda/(n+\lambda) \\ \omega_{\mathrm{c}}^{(0)}=\lambda/(n+\lambda)+(1-\alpha^2+\beta) \\ \omega_{\mathrm{m}}^{(i)}=\omega_{c}^{(i)}=\lambda/2(n+\lambda),\ i=1,2,...,2n \\ \lambda=n(\alpha^2-1) \end{cases} \tag{7}$$

where ω_{m} and ω_{c} are the weights of the first-order and second-order statistical properties, respectively. Constant α determines the spread of sigma points around the state estimation $\hat{x}$, and constant β is used to merge part of the prior knowledge of the distribution of state vector x.

(3) Sampling points

According to Eq. (6) and Eq. (7), to obtain a set of Sigma points as follows,

$$x^{(i)}(k\,|\,k)=\begin{cases}\hat{x}(k\,|\,k)\\ \hat{x}(k\,|\,k)+\sqrt{(n+\lambda)P(k\,|\,k)}\\ \hat{x}(k\,|\,k)-\sqrt{(n+\lambda)P(k\,|\,k)}\end{cases},\quad i=0,1,...,2n$$

(4) State prediction

$$x^{(i)}(k+1\,|\,k)=f[x^{(i)}(k\,|\,k)]+w(k),\quad i=1,2,...,2n+1$$

$$\hat{x}(k+1\,|\,k)=\sum_{i=0}^{2n}\omega^{(i)}x^{(i)}(k+1\,|\,k)$$

$$P(k+1\,|\,k)=\sum_{i=0}^{2n}\omega^{(i)}[\hat{x}(k+1\,|\,k)-x^{(i)}(k+1\,|\,k)][\hat{x}(k+1\,|\,k)-x^{(i)}(k+1\,|\,k)]^{\mathrm{T}}+Q$$

(5) New Sigma points

$$x^{(i)}(k+1\,|\,k)=\begin{cases}\hat{x}(k+1\,|\,k)\\ \hat{x}(k+1\,|\,k)+\sqrt{(n+\lambda)P(k+1\,|\,k)}\\ \hat{x}(k+1\,|\,k)-\sqrt{(n+\lambda)P(k+1\,|\,k)}\end{cases},\quad i=1,2,...,2n+1$$

(6) Measurement prediction

$$z^{(i)}(k+1\,|\,k)=h[z^{(i)}(k\,|\,k)]+v(k),\quad i=1,2,...,2n+1$$

$$\hat{z}(k+1\,|\,k)=\sum_{i=0}^{2n}\omega^{(i)}z^{(i)}(k+1\,|\,k)$$

$$P_{z(k)z(k)}=\sum_{i=0}^{2n}\omega^{(i)}[z^{(i)}(k+1\,|\,k)-\hat{z}(k+1\,|\,k)][z^{(i)}(k+1\,|\,k)-\hat{z}(k+1\,|\,k)]^{\mathrm{T}}+R$$

$$P_{x(k)z(k)}=\sum_{i=0}^{2n}\omega^{(i)}[x^{(i)}(k+1\,|\,k)-\hat{z}(k+1\,|\,k)][z^{(i)}(k+1\,|\,k)-\hat{z}(k+1\,|\,k)]^{\mathrm{T}}$$

(7) Update

$$K(k+1)=P_{x(k)z(k)}P^{-1}{}_{z(k)z(k)}$$

$$\hat{x}(k+1\,|\,k+1)=\hat{x}(k+1\,|\,k)+K(k+1)[z(k+1)-\hat{z}(k+1\,|\,k)]$$

$$P(k+1\,|\,k+1)=P(k+1\,|\,k)-K(k+1)P_{z(k)z(k)}K^{\mathrm{T}}(k+1)$$

(8) Prediction

$$x(k\,|\,k-1)=A(k)x(k-1\,|\,k-1)$$

$$P(k\,|\,k-1)=A(k)P(k-1\,|\,k-1)A^{\mathrm{T}}(k)+Q$$

As a nonlinear estimation method, EKF is widely used in state estimation, but this approach has some shortcomings such as the requiring state dynamics to be different and susceptibility to divergence in state estimate (Wu et al., 2010). The UKF adopts the nonlinear model instead of linearization directly. According to a series of deterministic samples, it improves the filtering effect of nonlinear system by approximating the posterior probability density of state and the probability distribution of nonlinear functions. What is more, the UKF has the second-order Taylor series expansion while EKF is accurate to the first order for arbitrary nonlinearity (Jung et al., 2014).

Particle Filter

According to a sequential Bayesian estimation framework, if the initial probability density function (PDF) of the state $p(x(0))$ is known, the posterior PDF $p(x(k) \mid z(1:k))$ of a state can be obtained through using a series of measurements at time k, and then the state estimation can be realized (Leng et al., 2012). It is assumed that initial PDF $p(x(0) \mid z(0)) = p(x(0))$. To obtain the posterior PDF $p(x(k) \mid z(1:k))$, two steps are performed as follows.

Step 1: State prediction

$$p(x(k) \mid z(1:k-1)) = \int p(x(k) \mid x(k-1)) p(x(k-1) \mid z(1:k-1)) dx(k-1)$$

Step 2: State update

$$p(x(k) \mid z(1:k)) = \frac{p(z(i) \mid x(k))\, p(x(k) \mid z(1:k-1))}{\int p(z(k) \mid x(k)) p(x(k) \mid z(1:k-1)) dx(k)}$$

By applying sequential importance sampling (Ibrahim et al., 2015), the estimation of

$p(x(k) \mid z(1:k))$ can be achieved by the recursive propagation of weights,

$$p(x(k) \mid z(1:k)) \approx \sum_{k=1}^{N} \omega^i(k) \delta(x^i - x^i(k)) \tag{8}$$

where $\omega^i(k)$ is the weight of the k-th particle at time i, and $\delta(x)$ is the Dirac-delta function by letting $x(k) \sim q(x)$ be an importance density.

There is a fatal disadvantage in existence with PF, i.e., weight degeneration (Han et al., 2016). The phenomenon is that one of the normalized weights inclines to 1, and others become inappreciable. The weight degeneration implies that a great deal of calculation is wasted on particle updating, which have a little contribution to the approximation of the posterior probability density. In order to prevent the weight degradation, currently, resampling is the main approach to solve the problem, and it is applied to discard particles with low weights and propagate particles with high weights.

The resampling method used in basic PF is based on probability accumulation. It is assumed that $\{x^i(k)\}_{k=1,\ldots,N}$ is the state sequence before resampling and $\{\tilde{x}^i(k)\}_{k=1,\ldots,N}$ is the one after resampling. The particle set of the posterior distribution of the target state is assumed to be $\{x^i(k-1), \omega^i(k-1)\}_{i=1}^{N}$ at time k-1. Then the specific implementation steps of the PF algorithm are as follows (Zuo et al., 2016):

1) Importance sampling

2) **For** $i = 1,2,\ldots,N$

3) $\tilde{x}^i(k) \sim q(\tilde{x}^i(k) \mid \tilde{x}^i(k-1), z(k))$

4) According to the current observation $z(k)$, the weights of each particle $\{\tilde{x}^i(k)\}_{i=1}^{N}$ are calculated as follows,

5) $\tilde{\omega}^i(k) = \tilde{\omega}^i(k-1)\dfrac{p(z(k)\,|\,\tilde{x}^i(k))p(\tilde{x}^i(k)\,|\,x^i(k-1))}{q(\tilde{x}^i(k)\,|\,\tilde{x}^i(k-1), z(k))}$

6) Normalized particle weights $\tilde{\omega}^i(k) = \tilde{\omega}^i(k) / \sum_{j=1}^{N} \tilde{\omega}^j(k)$

7) Resampling. The effective sample number N_{eff} is computed as follows,

$N_{eff} = 1 / \sum_{j=1}^{N} (\tilde{\omega}^i(k))^2$

8) **If** $N_{eff} < N_{th}$

9) Resampling particle $\{\tilde{x}^i(k), \tilde{\omega}^i(k)\}_{i=1}^{N}$ to obtain a new particle set:

$\{x^i(k), 1/N\}_{i=1}^{N}$

10) **Else** $\{x^i(k), \omega^i(k)\}_{i=1}^{N} = \{\tilde{x}^i(k), \tilde{\omega}^i(k)\}_{i=1}^{N}$

11) **End If**

12) State estimation: $\hat{x}(k) = \sum_{i=1}^{N} \tilde{\omega}^i(k) x^i(k)$

13) **End For**

Reconstruction of defect profile

Establishment of state-space model

Based on the foregoing analysis, the primary purpose of this paper is to reconstruct the defect profile from MFL signals. The reconstruction process can be described as a tracking problem by establishing the state-space model.

In this study, at location k, it is assumed that $x(0:k) = \{x(0), x(1), ..., x(k)\}$ is the sequence of defect depth, denoting the state transition model of state-space model, and $z(0:k) = \{z(0), z(1), ..., z(k)\}$ is the inspected MFL signal, representing the measurement model.

The process of the 2D defect profile reconstruction of MFL testing is shown in Figure 2. The state transition probabilities were selected such as to allow a higher probability of staying at the same depth and lower probabilities of the profile transitioning to other depths. When solving the problem of profile reconstruction, the defect profile is predicted from measurement sequences on test data in this paper.

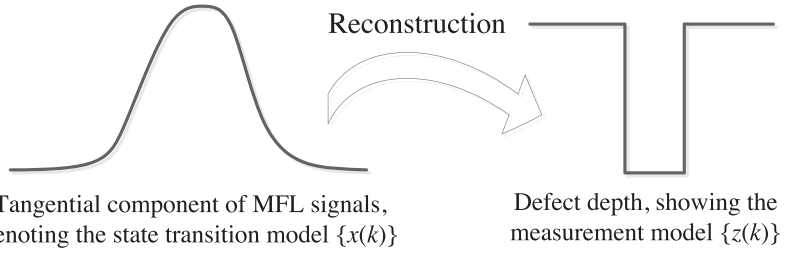

Figure 2. Defect depth reconstruction from MFL signals.

Establishment of MFL testing

In this paper, the two-dimensional MFL data simulated by finite element method software ANSYS are used to evaluate the performance of the profile reconstruction problem. To acquire the data of both the state transition model

and the measurement model, an experiment is carried out on rectangular cracks to achieve the MFL data and the true defect profile. The model of MFL testing is shown in Figure 3.

In order to apply experimental MFL signals, which are gained from the practical detection, to testing the method presented in Figure 3, a 2D finite element model is established in the same size and materials as the experimental one. In this experiment, the specimen adopts a solid sucker rod with a diameter of 19.05 mm, and the material property is made of X52 steel; its ***B-H*** curve is shown in Figure 4. The MFL testing of the defect is carried out by applying the double DC coils magnetization approach. The coils are composed of multilayer winding. The number of turns is 500; the inner diameter, the outer diameter, and the length are 17 mm, 48 mm, and 41 mm respectively. Rectangular defects are manufactured with different dimensions in the sucker rod.

The Hall sensor is selected to collect the MFL signals, the type is A1302, and its sensitivity is 1.3 mV/G. The experimental data is acquired after a denoising process.

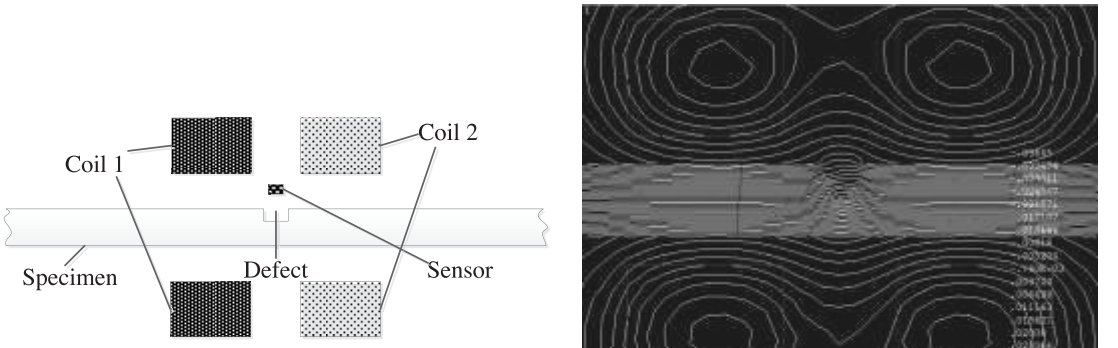

(a) MFL testing model **(b)** 2D model in ANSYS

Figure 3. 2D model of MFL testing.

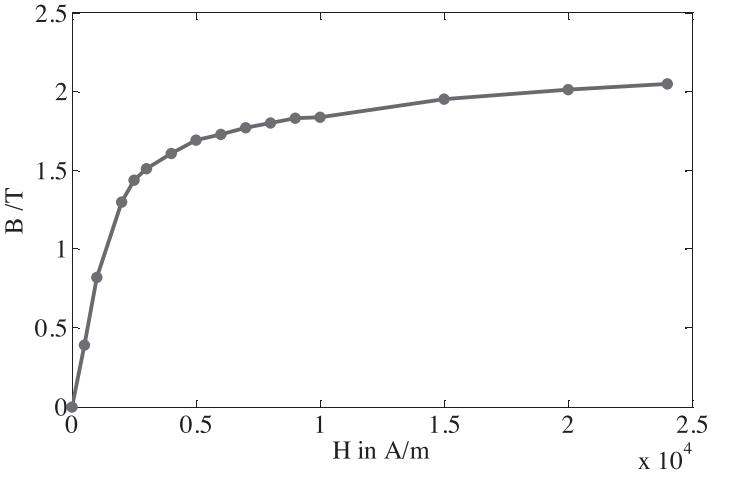

Figure 4. The ***B-H*** curve of X52.

RESULTS AND ANALYSIS

A state transition model is established according to the defect profile, and a measurement model is also built based on the inspected MFL signals. Three filter approaches are applied in achieving the reconstruction of defect depth. We introduce the root-mean-square error (*RMSE*) and signal to noise ratio (*SNR*) between the true and estimated profiles,

which are calculated to evaluate the performance of the three approaches. The definitions of *RMSE* and *SNR* are as follows:

$$RMSE = \sqrt{\frac{1}{N}\sum_{k=1}^{N}(x(k)-\hat{x}(k))^2} \tag{9}$$

$$SNR = 10\lg(\sum_{k=1}^{N}x^2(k) / \sum_{i=k}^{N}(x(k)-\hat{x}(k))^2) \tag{10}$$

Reconstruction of simulation data

The data used in defect profile reconstruction is generated by the use of the finite element model described above. To obtain the defect database, a multilevel flaw of rectangular cross section is machined in the test-piece, and the reconstruction of defect depth profile from MFL data is analyzed.

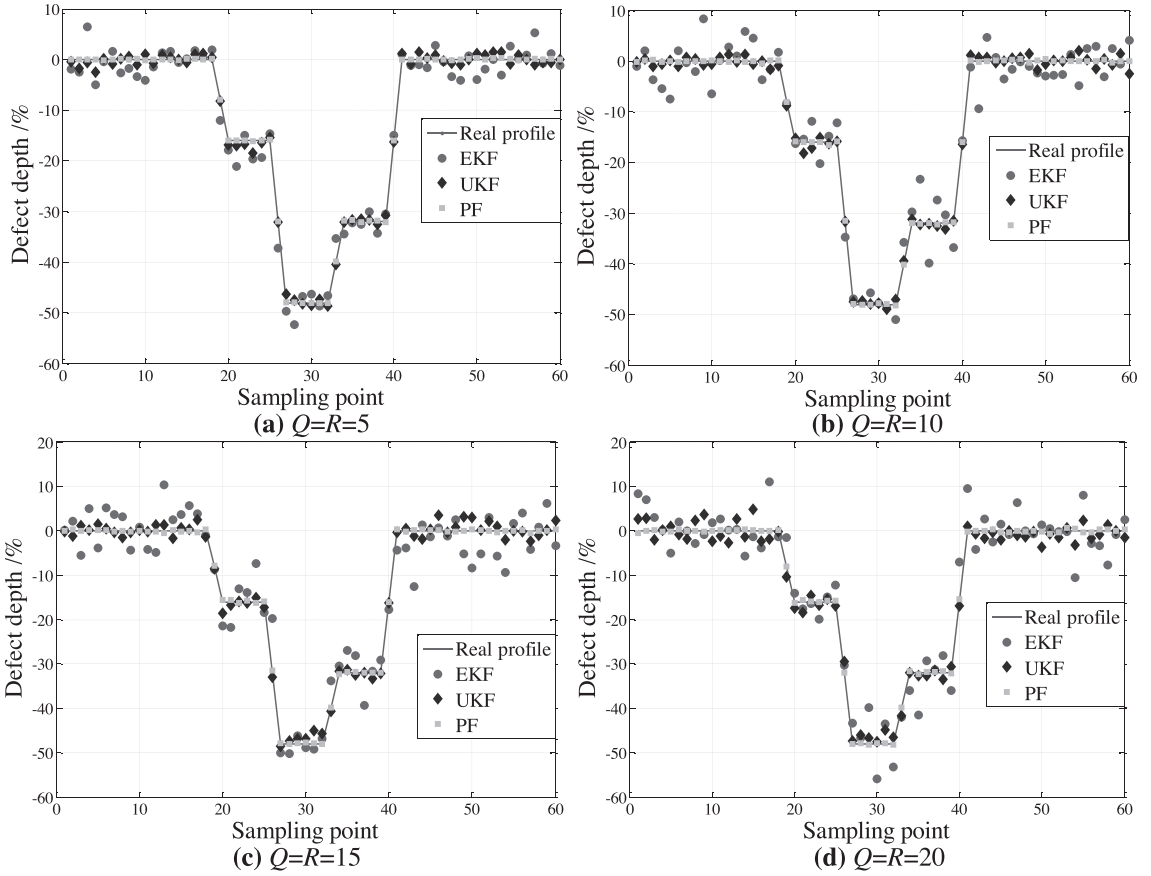

Figure 5. Comparison of the estimated profiles by EKF, UKF, and PF.

The reconstruction results of defect depth using EKF, UKF, and PF are shown in Figure 5. The reconstruction results with different variances of the process noise *Q* and measurement noise *R* are given in Fig.5 **(a)** to Fig.5 **(d)**. As can be seen, the three reconstruction methods can be realized in reconstructing the defect depth, but it can also be observed that the reconstruction effect of PF is far better than that of EKF and UKF.

Table 1. Performances of the three approaches.

Index	EKF	UKF	PF	Conditions
RMSE	2.6142	0.9088	0.1210	*Q*=5
SNR	17.7542	26.9314	44.4455	*R*=5
RMSE	3.6971	0.9132	0.1872	*Q*=10
SNR	14.7437	26.8895	40.6553	*R*=10
RMSE	4.7872	1.3823	0.2347	*Q*=15
SNR	12.4992	23.2887	38.6894	*R*=15
RMSE	5.4301	1.6234	0.2660	*Q*=20
SNR	11.4047	21.8922	37.6036	*R*=20

Table 1 lists the comparison of the reconstruction performances with different variances using the three reconstruction approaches. *RMSE* is used to measure the deviation between the observed value and the true value. If the value of *RMSE* is smaller, the reconstruction performance would be considered good, indicating that the actual profile approximates the estimated profile. *SNR* is the anti-interference ability of the reconstruction method for different noises (process noises and measurement noises). The greater its value, the stronger the anti-interference ability of the method. As shown in the table, reconstruction *RMSE* and *SNR* are different when the variances are diverse, but the reconstruction can be successfully completed as noise exists. In addition, *RMSE* increased and *SNR* decreased with increasing variances being observed from the table; meanwhile, the reconstruction performance of PF is better than that of the other two methods, possessing beautiful robustness.

Reconstruction of experimental data

Different from simulated MFL signals, the experimental MFL signals include noise that appears when the Hall sensor acquires the signals. In this experiment, a transverse defect is selected as the MFL testing object. We artificially carved a transverse defect in the sucker rod; the length is 2 mm, and the depth is 7.5 mm. To testify the validity of the three methods presented in this paper, taking the measured signals after denoising as the input measurement data, as depicted in Figure 6. It is assumed that the variances of process noise and measurement noise are equal to 15, so the reconstruction results can be achieved using the three reconstruction approaches, as shown in Figure 7.

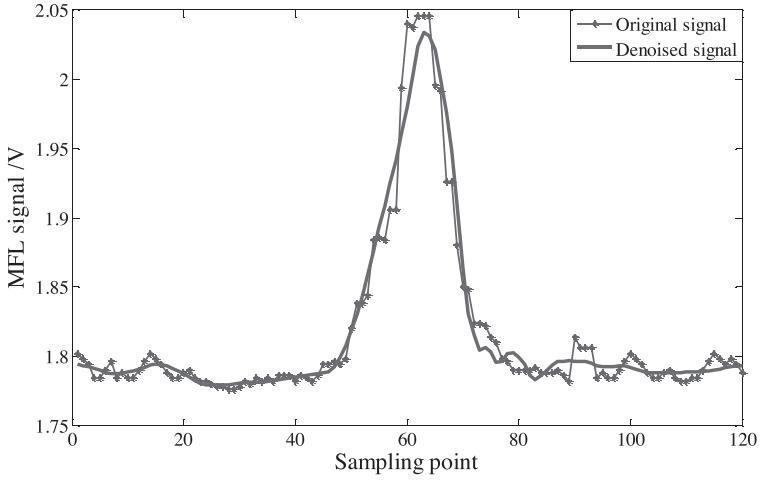

Figure 6. Tangential component of the experimental MFL signal.

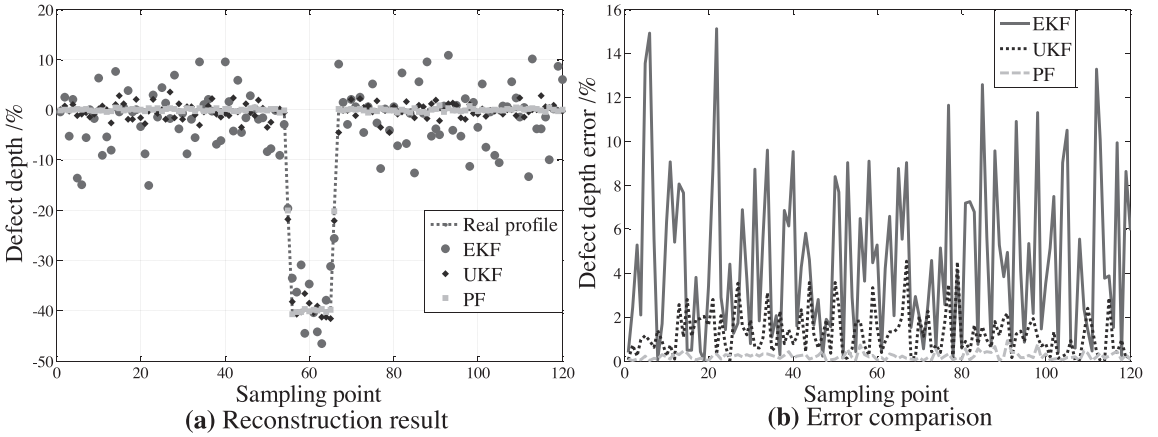

(a) Reconstruction result **(b)** Error comparison

Figure 7. Reconstruction result of defect depth from the experimental MFL signals.

The reconstruction results indicate that the three reconstruction methods can achieve the defect reconstruction from the experimental MFL signals, but the reconstruction performances are vastly different. In Fig.7 **(b)**, the result of the PF is obviously higher than that of the other methods. Figure 8 presents the changing trends of the evaluation indexes *RMSE* and *SNR* under different variances of process noise and measurement noise. It can be seen that *RMSE* increases with the increase of variances, and *SNR* decreases with the increase of variances. The changing trends demonstrate that the reconstruction performance of PF is optimal with good stability.

Figure 9 depicts the calculation time of the three methods under different variances of process noise and measurement noise. It can be noticed that the PF approach has the longest computation time, which is still within an acceptable range, and EKF method requires the least time.

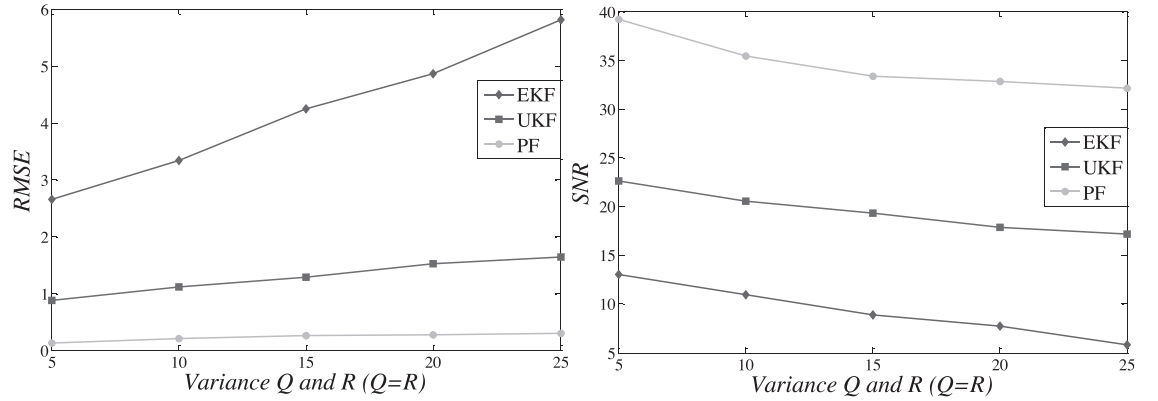

(a) *RMSE* **(b)** *SNR*

Figure 8. Changes of RMSE and SNR with different variances.

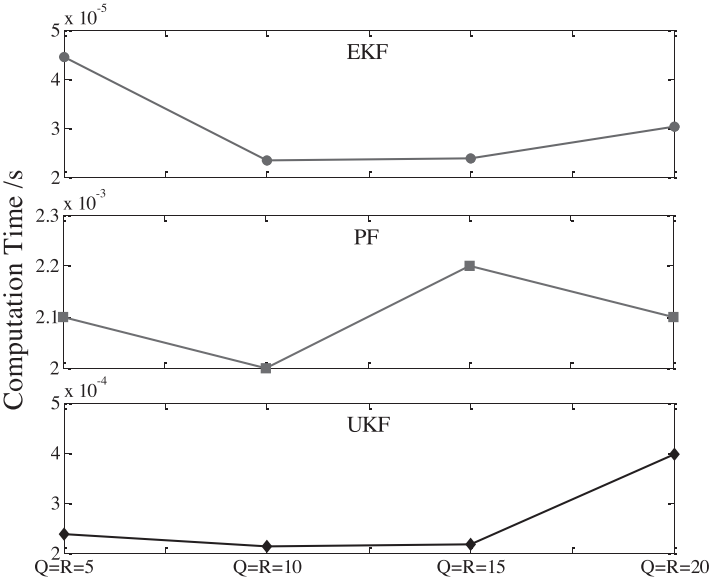

Figure 9. Calculation time of the three methods.

From the above reconstruction results, it is clearly true that the reconstruction performance of PF is better than that of EKF and UKF, and it has good robustness and stability; however, PF method has the longest computation time. In order to further discuss the reconstruction effect of PF, the reconstruction result from the experimental MFL signals is analyzed when the variances of process noise and measurement noise are up to 50, and the result is shown in Figure 10. From Figure 10, the reconstruction of defect depth from the detected MFL signals indicates that the PF approach is capable of producing reasonably accurate results, even in the presence of larger noise. From both simulation and experimental results, this work concludes that the PF approach has better performance than the EKF and UKF.

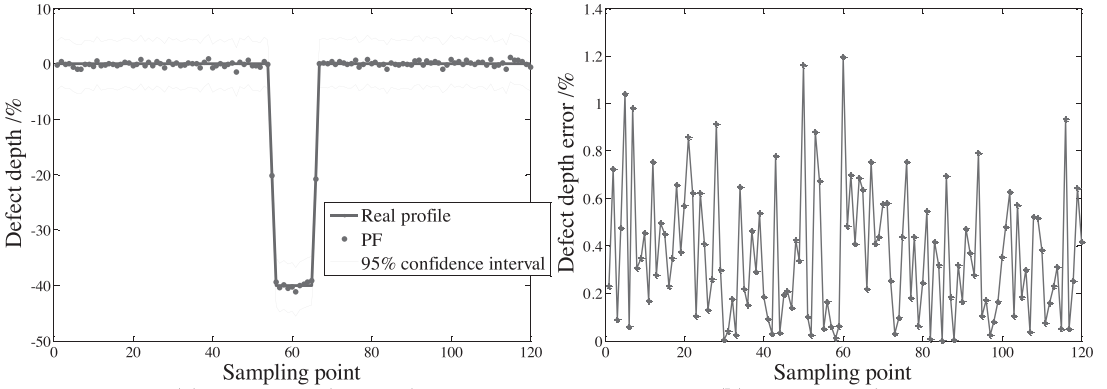

(a) Reconstruction result **(b)** Reconstruction error

Figure 10. Reconstruction performance using PF method.

CONCLUSION

This paper applies three approaches, EKF, UKE, and PF, to achieve the 2D defect profile reconstruction from MFL signals. The defect depth reconstruction is carried out from two aspects of simulation data and experimental data, and the reconstruction performances of the three methods are compared through the evaluation indexes, i.e., *RMSE* and *SNR*. The results indicate that the *RMSE* increases and *SNR* decreases as the variances of the process and

measurement noises increase, and the three methods introduced in this paper can be achieved in reconstructing the defect profile. Meanwhile, the reconstruction effect of PF is superior to that of EKF and UKF due to the good accuracy and robustness, and PF is a more effective and feasible approach to solve the inverse problems.

REFERENCES

Astroza, R., Luan, T.N. & Nestorović, T. 2016. Finite element model updating using simulated annealing hybridized with unscented Kalman filter. Computers & Structures, **177**:176-191.

Bonnet, V., Dumas, R., Cappozzo, A., Joukov, V. & Daune, G. 2016. A constrained extended Kalman filter for the optimal estimate of kinematics and kinetics of a sagittal symmetric exercise. Journal of Biomechanics.

Bressel, M., Hilairet, M., Hissel, D. & Bouamama, B.O. 2015. Extended Kalman filter for prognostic of proton exchange membrane fuel cell. Applied Energy, **164**(2016):220-227.

Cang, W. & Yang, H. 2015. Estimation of catalytic activity using an unscented Kalman filtering in condensation reaction. Chinese Journal of Chemical Engineering, **23**(12):1965-1969.

Delgado-Aguiñaga, J.A., Besancon, G., Begovich, O. & Carvajal, J.E. 2016. Multi-leak diagnosis in pipelines based on extended Kalman filter. Control Engineering Practice, **49**:139-148.

Feng, J., Lu, S., Liu, J. & Li, F. 2017. A sensor liftoff modification method of magnetic flux leakage signal for defect profile estimation. IEEE Transactions on Magnetics, **53**(7).

Gonzales, C. & Dubuisson, S. 2015. Combinatorial resampling particle filter: an effective and efficient method for articulated object tracking. International Journal of Computer Vision, **112**(3):255-284.

Gurung, H. & Banerjee, A. 2016. Self-sensing shape memory alloy wire actuator based on unscented Kalman filter. Sensors & Actuators A: Physical **251**:258-265.

Han, W., Xu, J., Zhou, M., Tian, G. & Wang, P. 2016. Cuckoo search and particle filter-based inversing approach to estimating defects via magnetic flux leakage signals. IEEE Transactions on Magnetics, **52**(4):1-11.

Ibrahim, A., Zabri, A. & Nakahata, K. 2015. Identification of elastic parameters of an inclusion by a particle filter using ultrasonic waves. International Journal of Mechanical and Materials Engineering, **10**(1):10-23.

Jung, K., Kim, J., Jung, E. & Kim, S. 2014. Positioning accuracy improvement of laser navigation using UKF and FIS. Robotics & Autonomous Systems, **62**(9):1241-1247.

Kandroodi, M.R., Araabi, B.N., Bassiri, M.M. & Ahmadabadi, M.N. 2017. Estimation of depth and length of defects from magnetic flux leakage measurements verification with simulations, experiments, and pigging data. IEEE Transactions on Magnetics, **53**(3):1-10.

Khan, T. & Ramuhalli, P. 2008. A recursive Bayesian estimation method for solving electromagnetic nondestructive evaluation inverse problems. IEEE Transactions on Magnetics, **44**(7):1845-1855.

Kumar, S., Prakash, J. & Kanagasabapathy, P. 2011. A critical evaluation and experimental verification of Extended Kalman Filter, Unscented Kalman Filter and Neural State Filter for state estimation of three phase induction motor. Applied Soft Computing, **11**(3):3199-3208.

Leng, H.Z. 2012. Improved particle filter in data assimilation. Acta Physica Sinica, **61**(7).

Lindgren, E. 2015. Detection and 3-D positioning of small defects using 3-D point reconstruction, tracking, and the radiographic magnification technique. NDT & E International, **76**:1-8.

Li, Z., Wang, Y. & Liu, Z. 2016. Unscented Kalman filter-trained neural networks for slip model prediction, Plos One, **11**(7).

Li, H.W., Wang, J. & Su, H.T. 2011. Improved particle filter based on differential evolution. Electronics Letters, **47**(19):1078-1079.

Lu, S., Feng, J., Li, F. & Liu, J. 2017. Precise inversion for the reconstruction of arbitrary defect profiles considering velocity effect in magnetic flux leakage testing. IEEE Transactions on Magnetics, **53**(4).

Mukherjee, D., Saha, S. & Mukhopadhyay, S. 2013. Inverse mapping of magnetic flux leakage signal for defect characterization.

NDT & E International 54(3):198-208.

Nobrega, J.P. & Oliveira, A.L.I. 2015. Kalman filter-based method for online sequential extreme learning machine for regression problems. Engineering Applications of Artificial Intelligence, **44**:101-110.

Pan, S., Xiao, D., Xing, S., Law, S.S. & Du, P. 2016. A general extended Kalman filter for simultaneous estimation of system and unknown inputs. Engineering Structures, **109**:85-98.

Priewald, R.H., Magele, C., Ledger, P.D., Pearson, N.R. & Mason, J.S.D. 2013. Fast magnetic flux leakage signal inversion for the reconstruction of arbitrary defect profiles in steel using finite elements. IEEE Transactions on Magnetics, **49**(1):506-516.

Ramuhalli, P., Udpa, L. & Udpa, S.S. 2002. Electromagnetic NDE signal inversion by function-approximation neural networks. IEEE Transactions on Magnetics, **38**(6):3633-3642.

Ravan, M., Amineh, R.K.S., Koziel, S., Nikolova, N.K. & Reilly, J.P. 2010. Sizing of 3-D arbitrary defects using magnetic flux leakage measurements. IEEE Transactions on Magnetics, **46**(4):1024-1033.

Smorodinskii, Y.G., Novoslugina, A.P. & Shur, M.L. 2013. On the inverse problem of magnetostatics. Russian Journal of Nondestructive Testing, **49**(8):465-473.

Sun, Y., Liu, S., Ye, Z., Chen, S & Zhou, Q. 2016. A defect evaluation methodology based on multiple magnetic flux leakage (MFL) testing signal eigenvalues. Research in Nondestructive Evaluation, **27**(1):1-25.

Wu, Y. & Luo, X. 2010. Design of output data fusion soft sensor based on adaptive extended Kalman filtering algorithm. Ciesc Journal, **61**(10):2627-2635.

Xu, C., Wang, C., Ji, F. & Yuan, X. 2012. Finite-element neural network-based solving 3-D differential equations in MFL. IEEE Transactions on Magnetics, **48**(12):4747-4756.

Xu, C., Wang, C. & Ji, F. **2013.** KPLS-RWBFNN model for MFL 2D defect profile reconstruction. Nondestructive Testing and Evaluation. **28**(1):82-97.

Yuan, X., Wang, C., Zuo, X. & Hou, S. 2011. A method of 2D defect profile reconstruction from magnetic flux leakage signals based on improved particle filter, Insight-Non-Destructive Testing and Condition Monitoring, **53**(3):152-155.

Zhou, H., Deng, Z., Xia, Y. & Fu, M. 2016. A new sampling method in particle filter based on Pearson correlation coefficient. Neuro computing, **216**:208-215.

Zuo, J., Liang, Y., Zhang, Y. & Pan, Q. 2013. Particle filter with multimode sampling strategy. Signal Processing, **93**(11):3192-3201.